

The impact of (n,γ) reaction rate uncertainties on the predicted abundances of i-process elements with $32 \leq Z \leq 48$ in the metal-poor star HD94028

John E. McKay^{1,2,†}, Pavel A. Denissenkov,^{1,3,†*} Falk Herwig,^{1,3,†} Georgios Perdikakis^{3,4,5} and Hendrik Schatz^{3,5,6,†}

¹*Department of Physics & Astronomy, University of Victoria, Victoria, B.C., V8W 2Y2, Canada*

²*TRIUMF, 4004 Wesbrook Mall, Vancouver, B.C., V6T 2A3, Canada*

³*Joint Institute for Nuclear Astrophysics, Center for the Evolution of the Elements, Michigan State University, 640 South Shaw Lane, East Lansing, MI 48824, USA*

⁴*Department of Physics, Central Michigan University, Mt. Pleasant, Michigan 48859, USA*

⁵*National Superconducting Cyclotron Laboratory, Michigan State University, East Lansing, MI 48824, USA*

⁶*Department of Physics & Astronomy, Michigan State University, East Lansing, Michigan 48824, USA*

[†]*NuGrid Collaboration, <http://nugridstars.org>*

Accepted XXX. Received YYY; in original form ZZZ

ABSTRACT

Several anomalous elemental abundance ratios have been observed in the metal-poor star HD94028. We assume that its high [As/Ge] ratio is a product of a weak intermediate (i) neutron-capture process. Given that observational errors are usually smaller than predicted nuclear physics uncertainties, we have first set up a benchmark one-zone i-process nucleosynthesis simulation results of which provide the best fit to the observed abundances. We have then performed Monte Carlo simulations in which 113 relevant (n,γ) reaction rates of unstable species were randomly varied within Hauser-Feshbach model uncertainty ranges for each reaction to estimate the impact on the predicted stellar abundances. One of the interesting results of these simulations is a double-peaked distribution of the As abundance, which is caused by the variation of the ^{75}Ga (n,γ) cross section. This variation strongly anti-correlates with the predicted As abundance, confirming the necessity for improved theoretical or experimental bounds on this cross section. The ^{66}Ni (n,γ) reaction is found to behave as a major bottleneck for the i-process nucleosynthesis. Our analysis finds the Pearson product-moment correlation coefficient $r_P > 0.2$ for all of the i-process elements with $32 \leq Z \leq 42$, with significant changes in their predicted abundances showing up when the rate of this reaction is reduced to its theoretically constrained lower bound. Our results are applicable to any other stellar nucleosynthesis site with the similar i-process conditions, such as Sakurai’s object (V4334 Sagittarii) or rapidly-accreting white dwarfs.

Key words: nuclear reactions, nucleosynthesis, abundances, stars: abundances, stars: AGB and post-AGB

1 INTRODUCTION

Most of the chemical elements between Fe and Pb have been produced in the slow (s) or/and in the rapid (r) neutron-capture processes in stars or in stellar explosions. The neutron density in the s process is so low, $N_n \sim 10^8 \text{ cm}^{-3}$, that its path nearly follows the n-rich boundary of the valley of stability, outside of which the rates of β decay of unstable

isotopes exceed the n-capture rates (e.g., Busso et al. 1999; Käppeler et al. 2011). Because the s-process path is adjacent to the valley of stability, there are experimental nuclear physics data suitable for its modelling. On the contrary, the neutron density in the r process is so high, $N_n \sim 10^{20} \text{ cm}^{-3}$ (e.g., Thielemann et al. 2011), that its path approaches the neutron drip line and involves n-rich unstable isotopes with much less certain n-capture rates from theory. Therefore, the r-process nucleosynthesis is often taken into account in a chemical composition analysis of peculiar stars is by using

* E-mail: pavelden@uvic.ca

as templates heavy-element abundance patterns observed in stars that are empirically robustly determined to have been enriched only by an r-process source (e.g., Roederer et al. 2014a).

Roederer et al. (2016) tried to reproduce the anomalous heavy-element abundance distribution in the metal-poor star HD94028 ($[\text{Fe}/\text{H}]^1 = -1.6$) by a superposition of s- and r-process enrichments, using the s-process yields from the low-metallicity asymptotic giant branch (AGB) models of Karakas et al. (2014) and Shingles et al. (2015) and the r-process abundances from the star HD108317 measured by Roederer et al. (2012) and Roederer et al. (2014b), but they did not succeed. In particular, they were not able to explain the high $[\text{As}/\text{Ge}]$ and low $[\text{Se}/\text{As}]$ abundance ratios accompanied by the high $[\text{Mo}/\text{Fe}]$ and $[\text{Ru}/\text{Fe}]$ in that star. After considering possible contributions from other stellar nucleosynthesis sources, such as the weak r-process, neutron- or proton-rich neutrino winds and α -rich freezeout in core-collapse supernovae (SNe), electron-capture SNe, and the s process in fast-rotating massive stars, Roederer et al. (2016) came to the conclusion that the best fit to the distribution of the heavy-element abundances in HD94028 is obtained assuming that the s- and r-process abundances are complemented by abundances of the elements with $Z < 50$ produced in a weak intermediate (i) n-capture process, because only the latter seems to be able to provide the observed $[\text{As}/\text{Ge}] \approx +0.99$, $[\text{Se}/\text{As}] \approx -0.16$ and $[\text{Mo}/\text{Fe}] \approx +0.97$.

The i process in stars was first proposed by Cowan & Rose (1977). It occurs when H is ingested into a He convective zone at its top by some boundary mixing mechanisms, e.g. by the Kelvin-Helmholtz instability, with convection in the zone driven by He burning at its bottom. While the ingested H is being transported by convection to the deeper layers with an increasing temperature, it reacts with the abundant ^{12}C nuclei via $^{12}\text{C}(p,\gamma)^{13}\text{N}$ at a depth where this reaction becomes as fast as convective mixing. The radioactive ^{13}N decays to ^{13}C , while being carried further down to the bottom of the convective zone, because its half-life of 9.96 min is comparable to the convective overturn timescale. Finally, at the bottom, where the temperature is the highest, neutrons are released via $^{13}\text{C}(\alpha,n)^{16}\text{O}$. For the H ingestion rates $\dot{M}_{\text{ing}} \sim 10^{-12} - 10^{-9} M_{\odot} \text{ s}^{-1}$, estimated for convective He-shell flashes on CO white dwarfs from both 1D stellar evolution models and 3D hydrodynamic simulations, the i-process neutron density, that is proportional to \dot{M}_{ing} but also depends on the metallicity $[\text{Fe}/\text{H}]$, varies from $N_n \sim 10^{13} \text{ cm}^{-3}$ to $N_n \sim 10^{16} \text{ cm}^{-3}$, i.e. it is intermediate between the values characteristic of the s- and r-processes (Herwig et al. 2011, 2014a; Denissenkov et al. 2017, 2019).

The i-process action in a real star had most likely been witnessed by Asplund et al. (1999) in the post-AGB star Sakurai’s object (V4334 Sagittarii) when it experienced a very late thermal pulse of its He shell (Herwig et al. 2011). Possible indirect signatures of the i process are the anomalous heavy-element abundance distributions in the carbon-enhanced metal-poor (CEMP) r/s stars (Bertolli et al. 2013; Dardelet et al. 2014; Hampel et al. 2016; Denissenkov et al.

2019), the Pb deficiency in low-metallicity post-AGB stars (Lugaro et al. 2015), the high $[\text{Ba}/\text{La}]$ ratios in young open clusters (Mishenina et al. 2015), and the anomalous isotopic abundances in some presolar meteoritic grains (Jadhav et al. 2013; Fujiya et al. 2013; Liu et al. 2014). Stellar evolution theory predicts that, besides the H-ingesting He-shell flash convection on white dwarfs, the i process may also occur in metal-poor low-mass thermally-pulsing AGB stars (Lugaro et al. 2012), during a He-core flash in metal-poor RGB stars (Campbell et al. 2010), in super-AGB stars (Jones et al. 2016), and in Population-III massive stars when their H- and He-burning shells merge (Clarkson et al. 2019; Banerjee et al. 2018).

In this work, we investigate the robustness of the weak i-process elemental abundances and their ratios that are proposed to contribute to the anomalous chemical composition of the star HD94028. The predicted abundances are affected by uncertainties of the (n,γ) reaction rates for the unstable isotopes involved in this nucleosynthesis. By “weak” with typical neutron exposure $\tau \sim 1$ we mean an i process that, in spite of having a high neutron density, does not reach a large neutron exposure (time-integrated neutron flux), e.g. because it is terminated by the violent, global, non-radial instability that can be induced by H ingestion into the He-shell convection (Herwig et al. 2014b), as probably happened in Sakurai’s object Herwig et al. (2011). As a result of this “weakness” (a low neutron exposure), only the first n-capture peak elements (those with the neutron number close to the magic one $N = 50$) are produced in a significant amount by the weak i process. We employ the same computational methods and analysis tools that Denissenkov et al. (2018) (hereafter, Paper I) used in a similar study of i process producing the first peak elements observed in Sakurai’s object. Unlike in Paper I, we do not know the i-process site that contributed to the composition of HD94028. Therefore, we have to use a site-independent one-zone model with the temperature T , density ρ and initial chemical composition adjusted to mimic the i-process physical conditions appropriate for this case, like it was done by Roederer et al. (2016). We also deploy constant neutron-density equilibrium models that are independent of the neutron-source reactions.

2 METHODS

2.1 The benchmark simulation

For the one-zone simulations of the i process nucleosynthesis we use the NuGrid code *ppn* (Pignatari et al. 2016) with the same fixed temperature $T = 2 \times 10^8$ K and density $\rho = 10^4 \text{ g cm}^{-3}$ as in Paper I. The initial chemical composition is prepared using the solar system abundances of Asplund et al. (2009) scaled to the metallicity of the star HD94028 ($[\text{Fe}/\text{H}] = -1.6$), assuming that the α -element abundances are enhanced with the mean value of $[\alpha/\text{Fe}]$ equal to +0.4. The initial mass fraction of ^{12}C is increased to $X(^{12}\text{C}) = 0.5$ to be close to the values found in He-flash convective zones. We also reduce the initial hydrogen abundance to the value of $X(^1\text{H}) = 0.2$ adjusted to guarantee that the neutron density will reach the values of $N_n = 10^{13} - 10^{16} \text{ cm}^{-3}$ typical for the i process. The abundance of ^{16}O is adjusted accordingly to achieve the required metallicity. As

¹ We use the standard spectroscopic notation $[\text{A}/\text{B}] = \log_{10}(N(\text{A})/N(\text{B})) - \log_{10}(N_{\odot}(\text{A})/N_{\odot}(\text{B}))$, where $N(\text{A})$ and $N_{\odot}(\text{A})$ are abundances of an element A in a star and the Sun.

the comparison with the equilibrium models show, the details of these initial conditions do not impact the conclusions of this study.

The **ppn** simulations are run until the predicted nucleosynthesis yields match the observed abundances as well as possible. At this time, the high N_n phase would have ended because of hydrodynamic feedback from the $^{12}\text{C}(p, \gamma)^{13}\text{N}$ reaction. The final abundances obtained in **ppn** simulations have to be allowed to decay for a reasonably long time, say 1 Gyr, after which they may mix with some background abundances that are not necessarily equal to the initial abundances assumed for the star HD94028 (see Appendix A).

Our one-zone simulations of i-process nucleosynthesis use the full **ppn** network of ~ 5200 isotopes and ~ 67000 nuclear reactions. The reaction rates in the default network are taken from several sources that are all referenced in Paper I. The NuGrid input physics module provides a possibility to increase or decrease any included reaction rate by changing its multiplication factor f_i from the default value $f_i = 1$. This option is used in our Monte Carlo simulations of the impact of reaction rate uncertainties on the predicted abundances.

The benchmark one-zone simulation uses the above described **ppn** code setup with $f_i = 1$ and runs until its predicted decayed elemental abundances match, as well as possible, those observed in HD94028.

2.2 Reaction Rates & Maximum Variation Factors

The abundances obtained in the benchmark simulation depend on the (n, γ) reaction rates for unstable isotopes. Most of these (n, γ) rates in the default setup of the **ppn** code come from the JINA REACLIB v1.1 library (Cyburt et al. 2010) that recommends theoretical values calculated using the Hauser-Feshbach model code NON-SMOKER (Rauscher & Thielemann 2000). However, different Hauser-Feshbach models predict different (n, γ) rates for a same unstable isotope (e.g., see Fig. 5 in Bertolli et al. 2013), which therefore makes these rates quite uncertain. To take these uncertainties into account, we follow the same procedure as in Paper I. First, we use charts of n-capture reaction fluxes at the maximum neutron density obtained in the benchmark simulation to select those unstable isotopes whose (n, γ) reaction rate variations can affect the predicted abundances. For each of these isotopes we find a set of (n, γ) rates r_i calculated with the Hauser-Feshbach code TALYS² (Bersillon et al. 2007) using 20 different combinations of the nuclear level density and γ ray strength function models listed in Table 1 of Paper I as input physics data. The rate uncertainty is assumed to be represented by the ratio of the largest to the lowest rate from this set, $v_i^{\max} = r_i^{\max}/r_i^{\min}$, that we call the rate's maximum variation factor. The 113 unstable isotopes selected for the uncertainty study in this work are displayed with their radiative n-capture rates' maximum variation factors in Figure 1.

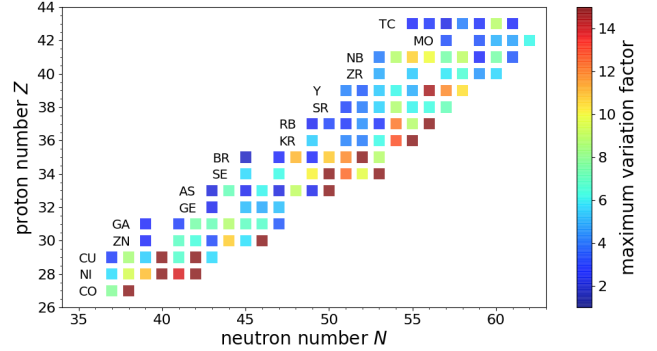


Figure 1. The unstable isotopes whose (n, γ) reaction rates were varied in this study and the maximum variation factors used for the rates. The maximum variation factors for ^{65}Co , ^{68}Ni , ^{70}Ni , ^{69}Cu , ^{71}Cu , ^{76}Zn , ^{83}As , ^{84}Se , ^{87}Se , ^{87}Br , ^{91}Kr , and ^{93}Rb exceed the maximum value of $v_i^{\max} = 15$ assigned to the color map.

2.3 The Monte Carlo Simulations

Our reaction rate uncertainty study is based on Monte Carlo (MC) simulations in which we perform 10000 runs of the **ppn** code with initial setups that differ from the benchmark simulation only by different choices of the rate multiplication factors for the selected (n, γ) reactions. Each of the MC simulation runs uses a different set of these factors in which $f_i = (p/v_i^{\text{rand}}) + (1-p)v_i^{\text{rand}}$, where p is assigned a value of either 0 or 1 with equal probability, and v_i^{rand} is randomly selected from a uniform distribution between 1 and v_i^{\max} (Paper I).

3 RESULTS

3.1 One-zone simulations of the i process

Figure 2 shows how the neutron number density N_n changes with time in our benchmark simulation. It reaches a value of $\sim 10^{16} \text{ cm}^{-3}$ at its maximum, indicating an i-process activation. The final nucleosynthesis yields in the i process also depend on its duration t , or on the neutron exposure

$$\tau = \int_0^t N_n v_{\text{th}} dt,$$

where v_{th} is the thermal velocity of neutrons. The evolution of the neutron exposure in our benchmark simulation is also shown in Figure 2. In the weak i process the latter never reaches the values of $\tau \sim 10-100$ at which abundance ratios of neighbouring elements of the first ($N \approx 50$) and second ($N \approx 82$) n-capture peaks attain their equilibrium values.

In order to identify a narrow interval of integration timesteps or intervals of t and τ in which the anomalous elemental abundance ratios observed in the star HD94028 are produced in the weak i process, we first examine the evolution of the isotopic progenitors of one of our main target elements As in Figure 3. We see that the abundances of the unstable isotopes ^{75}Ga and ^{75}Ge reach their peak values almost immediately after the 960th timestep (in 75 minutes). If we stop the benchmark simulation here and allow these isotopes to decay into the only stable As isotope ^{75}As , we will get its highest possible abundance, which we

² <http://talys.eu>

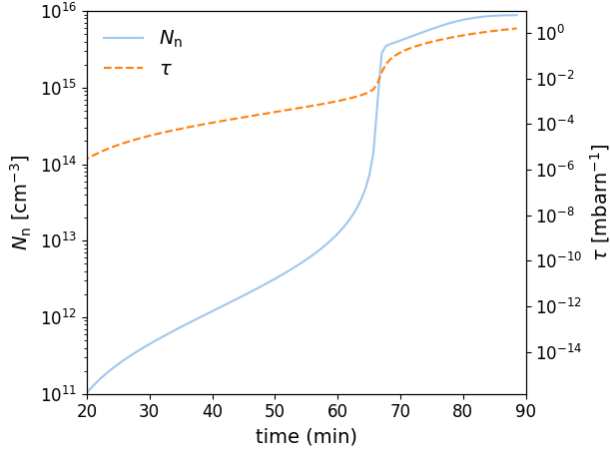


Figure 2. The evolution of the neutron number density and neutron exposure in our benchmark one-zone simulation.

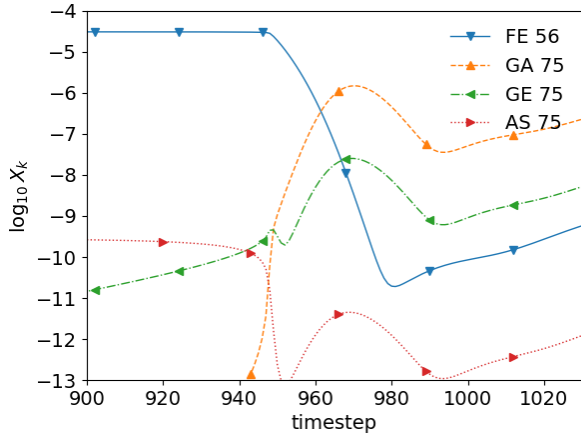


Figure 3. The evolution of the abundances of the two isotopes that decay into As and of the Fe seed in the benchmark simulation. The timestep 960 corresponds to 75 minutes of integration time.

need to explain the anomalously high $[As/Ge]$ ratio in the star HD94028.

Figure 3 also shows that after the ^{75}Ga and ^{75}Ge abundances have reached their peak values the most abundant of the Fe isotopes ^{56}Fe ceases being the main seed nucleus for the simulated i process. This is an artefact of the one-zone model. Moreover, the very presence of the peaks in the evolutionary profiles of the ^{75}Ga and ^{75}Ge abundances is seen to be caused by the depletion of the Fe abundance. In multi-zone simulations of the i process in a He convective zone the Fe abundance would not be depleted to such low values, because Fe destroyed at its bottom by n captures would be replenished by Fe brought there by mixing from the other parts of the convective zone, and a build-up of ^{75}Ga and ^{75}Ge could continue to overall larger values. However, at the moment when the neutron flux passes through these species

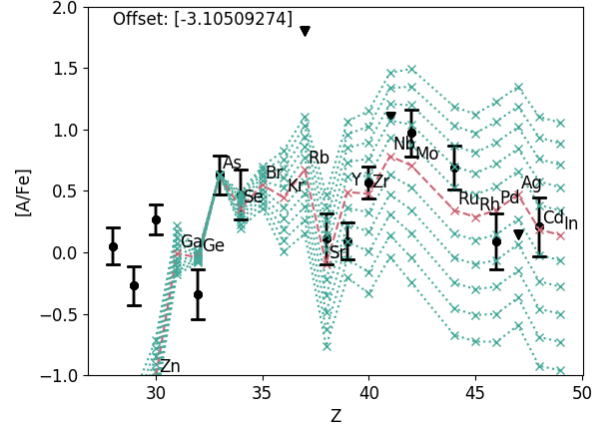


Figure 4. The distributions of $[A/Fe]_{\text{theor}}$ predicted by the benchmark simulation for the timesteps from 968 through to 978 (from the lower to upper curve) are compared with the observed values of $[A/Fe]$ from Roederer et al. (2016) to determine the best-fit timestep for the star HD94028. The 973rd timestep on the 85th minute has the minimum value of $\chi^2 = 18.0$ (the brown-dashed curve). The values of $[As/Fe]_{\text{theor}}$ are all pinned to the observed $[As/Fe]$ ratio (see Appendix A). The upside-down triangles are the upper limits.

they adopt their local equilibrium values. These are what we are seeking for to compare with the observed abundances.

Next, we use Figure 4 to determine a timestep at which the decayed and mixed elemental abundances predicted by the benchmark model best fit their corresponding i-process abundances derived by Roederer et al. (2016) for the star HD94028. With the predicted abundance of As pinned to its observed value the best-fit timestep turns out to be the 973rd one that corresponds to 85 minutes of integration time. At this time the calculated abundances $[A/Fe]_{\text{theor}}$ minimize

$$\chi^2 = \sum_{32 \leq Z \leq 48} \frac{([A/Fe]_{\text{obs}} - [A/Fe]_{\text{theor}})^2}{\sigma([A/Fe]_{\text{obs}})^2},$$

where Z is the proton number of an element A with available observed abundance $[A/Fe]_{\text{obs}}$ and corresponding error $\sigma([A/Fe]_{\text{obs}})$.

The normalization factor $d \approx -3.1\text{dex}$ (Offset in Figure 4) used to match the abundance pattern at As gives an indication of the fraction of i-process isotopes in the composition (see Appendix A).

A characteristic feature of an i-process is that its path band on a chart of nuclides involves only unstable isotopes that are two to eight neutron numbers away from the valley of stability (Figure 5). During the i process, especially large abundances are usually found for isotopes with neutron numbers close to the magic ones. In our case these are ^{84}Se , ^{85}Br and ^{86}Kr with $N = 50$ and $34 \leq Z \leq 36$. Large abundances also occur for the unstable Ge isotopes ($Z = 32$), ^{78}Ge , ^{79}Ge , & ^{80}Ge .

Of particular importance for this work are the large abundances of ^{74}Zn and ^{75}Ga ($Z = 30$ and 31), which are significantly higher than the subsequent neutron capture products ^{75}Zn and ^{76}Ga . The latter isotope is the main source of As. This indicated a significant bottleneck for the n-capture

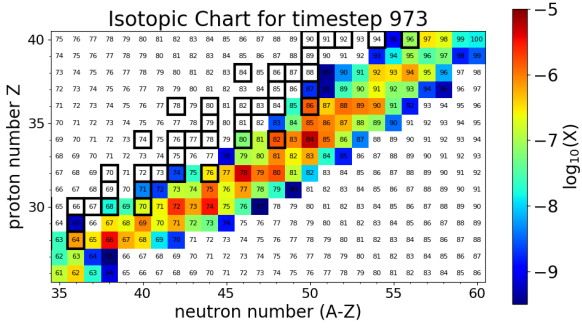


Figure 5. Undecayed isotopic abundances (mass fractions X) for the best-fit timestep 973 near the *i*-process nucleosynthesis peak.

reaction flux at this point. The Monte Carlo simulations confirm this (see Section 3.2).

A notable outlier is ^{66}Ni ($Z = 28$) that has a very high abundance compared to its surrounding isotopes. Its (n,γ) reaction product ^{67}Ni has a lower abundance which, combined with the two-day half-life of ^{66}Ni , signifies that ^{66}Ni also represents an important *i*-process bottleneck deserving a special attention.

3.2 The Monte Carlo simulations

The Monte Carlo (MC) simulations produce 10000 sets of the elemental and isotopic abundances from the timestep 973 and subsequent 1 Gyr beta decay that provides the best-fit of the theoretical to observed abundances for the benchmark model (Figure 4). Mixing with other material does not need to be considered here because we are only interested in finding correlations between the randomly varied reaction rate multiplication factors f_i and the predicted abundances (mass fractions) X_k . These correlations are evaluated using the Pearson product-moment correlation coefficient $r_P(f_i, X_k)$ (Equation (2) in Paper I).

Figure 6 shows the final distributions of $\log_{10}(X_k/X_{k,\odot})$ obtained in our MC simulation. Strong deviations from a Gaussian indicate the presence of important branching points on the *i*-process paths leading to the synthesis of isobars that decay into the same element. A prominent example of such a deviation is As whose MC abundances pile up in two distinct groups, one having the high mean abundance at a level of ~ 1 dex above the Ge abundances, as indicated by observations, and the other lying roughly on the same level with Ge. This is shown more clearly in Figure 7, together with the MC abundance distribution for Ge, which also shows a double peaked structure, albeit less pronounced. As we will show below, the bifurcation of the As abundance distribution is caused by the ^{75}Ga bottleneck.

Figure 8 shows the distributions of the Ga, Ge, As and Se abundances as functions of the multiplication factors for the ^{69}Cu , ^{72}Zn , ^{75}Ga and ^{78}Ge *n*-capture rates with which these abundances have the strongest correlations.

To identify all neutron capture rate uncertainties that affect the relevant elemental abundances, we have calculated the Pearson correlation coefficient for each of these elements

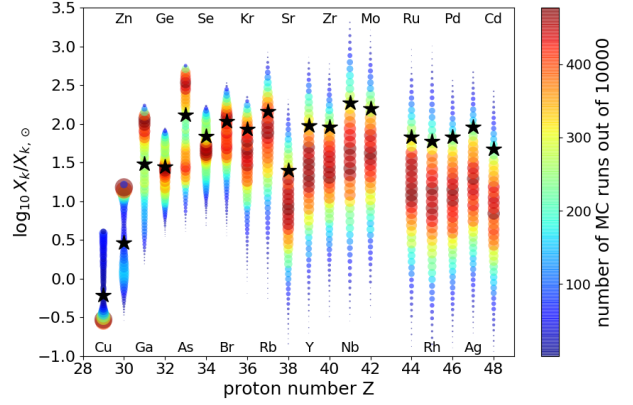


Figure 6. The distributions of the *i*-process elemental abundances generated in the Monte Carlo simulation by randomly varying (n,γ) reaction rates of the unstable isotopes that are displayed in Figure 1. The larger and redder circles correspond to a larger number of MC runs contributing to a given abundance. The black star symbols show the benchmark simulation abundances.

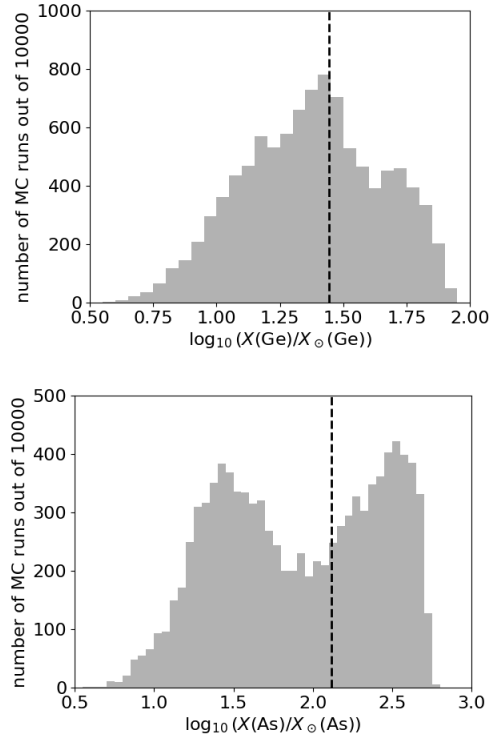


Figure 7. The Ge and As elemental abundance distributions from our Monte Carlo simulation. The abundances from the benchmark simulation are marked by black vertical dashed lines.

and for all the isotopes whose (n,γ) reaction rates were varied. Figure 9 shows the resulting correlations of the predicted Ga, Ge, As and Se abundances with the (n,γ) rate multiplication factor for ^{66}Ni and some other unstable isotopes. When examining all the *i*-process elements up to Mo ($Z = 42$), we find that $f(^{66}\text{Ni})$ positively correlates with

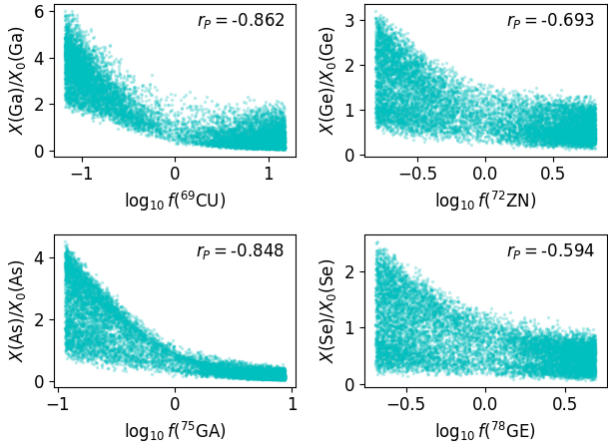


Figure 8. The distributions of the elemental abundances of Ga, Ge, As and Se as functions of the (n,γ) reaction rate multiplication factors for the selected isotopes of Cu, Zn, Ga and Ge for which the absolute magnitudes of the correlation coefficient are the largest (shown in the top-right corners of the panels).

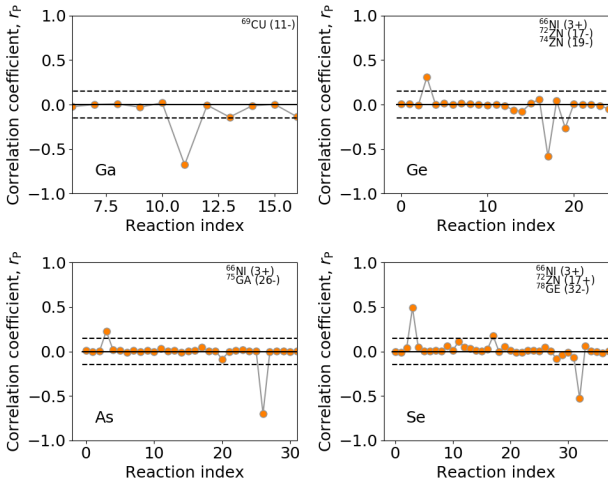


Figure 9. Correlation coefficients for the abundances of Ga (upper left), Ge (upper right), As (lower left), and Se (lower right) with reaction rate variations as functions of reaction index. Reaction indices with a sign of correlation and corresponding neutron capture target isotopes are given in the legends for the largest correlations.

the abundances of every element heavier than Ga (Table 1). This confirms that ^{66}Ni is also a major bottleneck isotope.

To investigate the impact of the ^{66}Ni neutron capture rate on the i -process reaction path band, we performed two additional calculations, where we only varied $f(^{66}\text{Ni})$ setting it to its maximum (9.4) and minimum (0.11) value, respectively. The results are shown in Figure 10. The maximum $f(^{66}\text{Ni})$ case shows very high isotopic abundances far along the i -process path band, while in the minimum case the (n,γ) reaction flux appears to be stuck at ^{66}Ni , resulting in a much enhanced accumulation of its abundance. Many

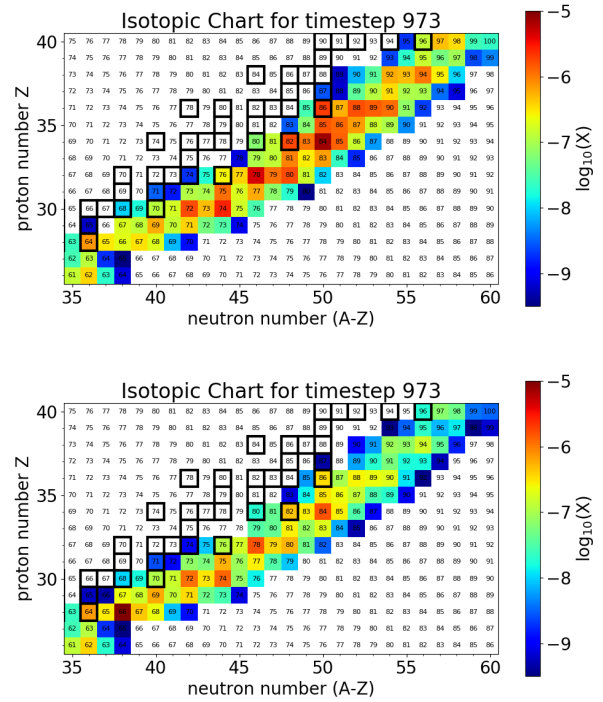


Figure 10. Isotopic abundances from the two additional ppn runs in which only the multiplication factor $f(^{66}\text{Ni})$ was switched between its maximum (top panel) and minimum (bottom panel) values constrained by the Hauser-Feshbach model computations.

isotopic abundances that had values of $\log_{10} X_k \geq -6$ in the benchmark simulation have dropped by $\sim 1-2$ orders of magnitude. This result is consistent with our correlation analysis and emphasizes the role of ^{66}Ni as a major bottleneck isotope. Replacing the default value of $f(^{66}\text{Ni}) = 1$ by $f(^{66}\text{Ni})_{\text{max}}$ and $f(^{66}\text{Ni})_{\text{min}}$ requires shifts of the best-fit timestep from the 973rd to the 972nd and 976th, respectively. These changes have an almost unnoticeable effect on Figure 10, therefore they do not affect our conclusion about $^{66}\text{Ni}(n,\gamma)$ being the major bottleneck reaction.

To show that it is the bifurcation of the (n,γ) reaction flux at the ^{75}Ga isotope and not at ^{66}Ni that is responsible for the double-peaked distribution of the As abundance, we have divided our MC simulation runs into two groups, one with $f(^{75}\text{Ga}) > 1$ and the other with $f(^{75}\text{Ga}) < 1$. Indeed this resulted in a separation of the As abundance distribution into two distinct peaks (top panel in Figure 11). On the other hand, a similar test for ^{66}Ni neutron capture rate only resulted in a shift of the double-peaked As abundance distribution to the higher abundance values (bottom panel in Figure 11). These tests show that although $^{66}\text{Ni}(n,\gamma)$ is the most important reaction for regulating the i -process nucleosynthesis paths in the $A = 75$ region of the chart of nuclides, the anomalously high abundance ratio $[\text{As}/\text{Ge}]$ in the star HD94028 is much more strongly affected by the uncertainty of the $^{75}\text{Ga}(n,\gamma)$ reaction rate that has to be reduced to increase $[\text{As}/\text{Ge}]$.

The major bottlenecks ^{66}Ni , ^{72}Zn , and ^{78}Ge lie on a sequence of nuclei with $Z = 26 + n$ and $N = 36 + 2n$ that for even n have particularly low Q -values for β^- decay ($<$

Reaction	Element	r_P (1-zone, 973rd timestep)	r_P (1-zone, 979th timestep)	r_P ($N_n = 10^{16} \text{ cm}^{-3}$)	r_P ($N_n = 10^{15} \text{ cm}^{-3}$)
^{66}Ni	Zn	-0.7793	-0.7108	-0.7497	-0.7948
	Ge	0.3079	-0.1255	0.1384	0.2286
	As	0.2298	-0.0583	0.1387	0.1969
	Se	0.4922	0.1412	0.4309	0.5210
	Br	0.4391	0.1340	0.3862	0.4240
	Kr	0.5031	0.3807	0.4938	0.6293
	Rb	0.4130	0.3387	0.3984	0.5215
	Sr	0.3601	0.3133	0.3475	0.4463
	Y	0.3093	0.2826	0.2929	0.4427
	Zr	0.4021	0.4435	0.3682	0.4646
	Nb	0.2906	0.2905	0.2706	0.3490
Mo	0.3583	0.4046	0.3174	0.3919	
^{69}Cu	Ga	-0.6776	-0.6071	-0.6500	-0.6022
^{72}Zn	Ge	-0.5842	-0.6450	-0.5892	-0.5943
^{75}Ga	As	-0.7021	-0.7291	-0.7040	-0.7725
^{78}Ge	Se	-0.5292	-0.7188	-0.5636	-0.5308

Table 1. The strongest correlations between the (n,γ) reaction rate variations and the i-process elemental abundances found in our MC simulations.

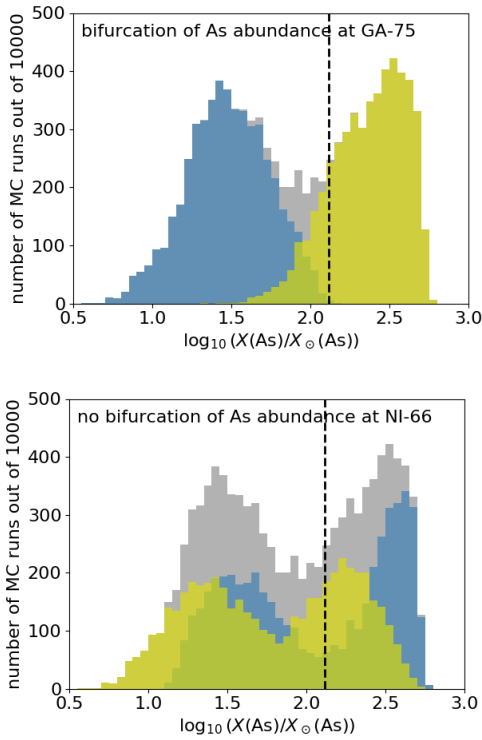


Figure 11. Top panel: the double-peaked distribution of the As elemental abundance in our MC simulation (grey) is decomposed into two isolated peaks (blue and yellow) when we divide the As abundances into two groups with $f(^{75}\text{Ga}) > 1$ and $f(^{75}\text{Ga}) < 1$. Bottom panel: a similar test with $f(^{66}\text{Ni})$ only shifts the distribution to the higher As abundances.

1 MeV) and at the same time relatively low Q -values for neutron capture ($\sim 5\text{--}6$ MeV). This results in both, long half-lives and slow neutron capture rates that make these

isotopes bottlenecks. As the i process begins mostly with the relatively abundant Fe isotopes ^{66}Ni is the first major bottleneck. For the odd n isotopes in this sequence the effect is less pronounced but still present — these are the isotopes ^{69}Cu , ^{75}Ga for which we also find some sensitivity.

Figure 6 shows that the neutron capture rate uncertainties have a tendency to reduce abundances below the benchmark values. Our analysis reveals that this is a cumulative effect in which the reaction $^{66}\text{Ni}(n,\gamma)$ plays an important but not defining role. When using the central values of the distributions for the comparison with observations, a fit with similar quality can still be obtained by increasing the integration time from 85 minutes (the 973rd timestep) to 89 minutes (the 979th timestep). Therefore, we have performed another MC simulation with the 979th timestep used as the final one and analyzed their results. This analysis has shown that all our main conclusions based on the results of the MC simulation with the 973rd final (best-fit) timestep remain true. For example, the values of the last four correlation coefficients in Table 1 have changed less than by 10% for the first three of them and by 36% for the fourth one compared to their values obtained in the first MC simulation (the last four rows in the 3rd and 4th columns).

We have not adjusted the integration time for each individual run of our MC simulation to get the best fit in order to estimate the “true” nuclear error bar because what we understand as nuclear uncertainty contribution to the abundances is the variation of abundances in respect to nuclear uncertainties for *fixed* astrophysical conditions.

For experimentalists it makes sense because they want to measure anything that affects abundances or the choice of stellar physics parameters. For example, if for a change of a bottleneck reaction one needs much longer exposure times to get the same abundances this should be flagged as something that needs a measurement even if it would result in the same abundance and would not pop up as important in the approach when the best-fit integration time is adjusted for individual MC runs.

For comparison with observations we want to include uncertainties of the astrophysical model and yes, there can then be correlations that we may miss in our approach, but we think that our simple definition of the nuclear component of the error is still sensible even if correlations are present. More importantly, we do not really have an astrophysical model for the case of HD94028, but a parametrized approach that is fitted, so there are no predictions of astrophysical parameters with errors. This is why it is tempting to use the individual integration time approach that would give us the nuclear uncertainties that need to be addressed to determine whether our parametrized approach can fit the observational data or not (which would not be uninteresting — though there are other parameters to adjust as well). Our approach, on the other hand, determines more generally the nuclear errors to expect in an i-process model that *fixes/predicts* astrophysical parameters (for example any future realistic stellar models) — we just use the parametrized approach to estimate the conditions in such a model — and it also flags reactions that affect the parameter choice.

The only concern one may have is that the sensitivities we determine depend sensitively on the astrophysical parameters, such as the exposure time. This is addressed by doing a second MC analysis at a different exposure time that can still fit the data within the nuclear uncertainty.

3.3 Simulations with a constant neutron density

To test the robustness of our predictions about the key role of the ^{75}Ga (n,γ) cross section in determining the production level of As and the role of the ^{66}Ni n-capture reaction as the major bottleneck for the synthesis of most of the i-process elements in the star HD94028, we have complemented our study with benchmark and MC one-zone simulations in which the neutron number density was kept constant and hydrogen burning was suppressed by assuming that its mass fraction $X = 0$, like it was done in the work of [Hampel et al. \(2016\)](#).

The results of these simulations are presented in Figure 12 and in the last two columns of Table 1. The figure shows that the values of $N_n < 10^{15} \text{ cm}^{-3}$ should not be considered because they result in too low $[\text{As}/\text{Ge}]$ and too high $[\text{Se}/\text{As}]$ abundance ratios accompanied by a too low $[\text{Ru}/\text{Fe}]$ abundance. As for the values of $N_n = 10^{15} \text{ cm}^{-3}$ and $N_n = 10^{16} \text{ cm}^{-3}$, the analyses of the results of MC simulations performed for them have led us to the same conclusions that we made using the one-zone model with the neutron density evolution profile shown in Figure 2, even the Pearson correlation coefficients have not changed much (Table 1).

4 SUMMARY AND CONCLUSIONS

Our study has been focused on the anomalously high $[\text{As}/\text{Ge}]$ abundance ratio in the metal-poor star HD94028. Following [Roederer et al. \(2016\)](#), we have assumed that this and the other abundance anomalies for the elements with $32 < Z < 48$ were contributed to this star by a weak i process that had occurred at an unknown stellar site.

To identify the isotopes whose (n,γ) reaction rate uncertainties have the strongest impact on the predicted As

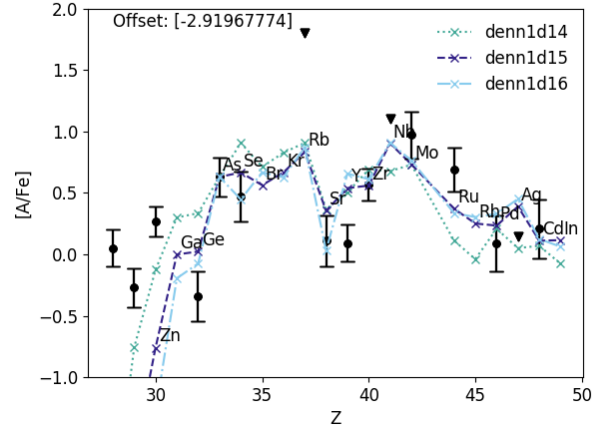


Figure 12. Same as the brown-dashed curve in Figure 4, but for the benchmark one-zone simulations with the constant neutron densities. The best-fit timesteps are 1183 (the 688th minute), 985 (the 96th minute) and 787 (the 13th minute) and their corresponding χ^2 values are 38.7, 19.8 and 22.5 from the lowest to the highest indicated values of N_n .

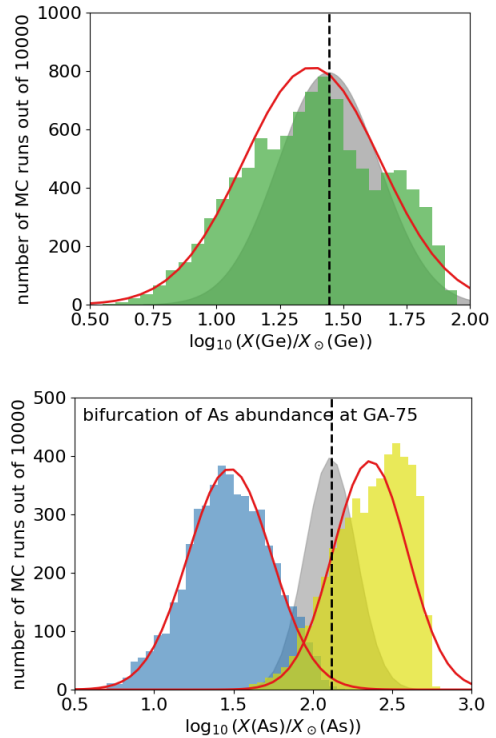


Figure 13. Comparison of the Gaussians fitted to the Ge and bifurcated As abundance distributions in the MC simulation (red curves) with the observed distributions of Ge and As in HD94028 also represented by the Gaussians (grey) with the mean values equal to the Ge and As abundances in the benchmark simulation and $\sigma([\text{Ge}/\text{Fe}]_{\text{obs}})$ and $\sigma([\text{As}/\text{Fe}]_{\text{obs}})$ estimated by [Roederer et al. \(2016\)](#).

abundance, we have performed Monte Carlo (MC) simulations in which the (n,γ) rates of 113 unstable isotopes that could affect the predicted i-process abundances in the star HD94028 were randomly varied within their minimum and maximum limits constrained by the Hauser-Feshbach model computations.

The MC simulations are based on the one-zone benchmark model of the i process nucleosynthesis for which we have selected the integration times (the final timesteps) providing the best fit of the predicted decayed elemental abundances to the i-process abundances in HD94028 derived by Roederer et al. (2016).

The analysis of the results of our MC simulations has revealed that the $^{75}\text{Ga}(n,\gamma)$ reaction has the strongest impact on the predicted As abundance. We have shown that the uncertainty of its rate leads to the bifurcation of the As abundance distribution. In the bottom panel of Figure 13 we have added Gaussians (red curves) fitting the two distinct As abundance distributions that are revealed when we divide the results of MC simulations into the groups with $f(^{75}\text{Ga}) < 1$ and $f(^{75}\text{Ga}) > 1$. We have also added a Gaussian (grey) with a mean value equal to the As abundance from the benchmark simulation (the black-dashed line) and the standard deviation $\sigma([\text{As}/\text{Fe}]_{\text{obs}})$ estimated for HD94028 by Roederer et al. (2016). The top panel shows a similar plot, but for Ge. This figure confirms the conclusion made by Denissenkov et al. (2018) that nuclear uncertainties of (n,γ) reaction rates relevant for i process are usually significant and overall similar to observational uncertainties. Given that $r_{\text{P}}(f(^{75}\text{Ga}), X(\text{As}))$ is negative (Table 1), the bottom panel of Figure 13 also shows that a reduction of the rate of the $^{75}\text{Ga}(n,\gamma)$ reaction would lead to the desired increase of $[\text{As}/\text{Ge}]$, while a significant increase of its rate would rule out the weak i process as one contributing to the abundance anomalies in the star HD94028.

It has also been shown that ^{66}Ni is the major bottleneck isotope that strongly affects most of the predicted abundances in the simulated i process. Therefore, experimental measurements of ^{75}Ga and ^{66}Ni n-capture rates would significantly improve our understanding of the i-process nucleosynthesis and its possible contribution to the elemental abundance anomalies in the star HD94028 and in other similar objects.

ACKNOWLEDGEMENTS

FH acknowledges funding from NSERC through a Discovery Grant. This research is supported by the National Science Foundation (USA) under Grant No. PHY-1430152 (JINA Center for the Evolution of the Elements). The authors thank Iris Dillmann, Barry Davids and Chris Ruiz for fruitful discussions of this problem. This research was enabled in part by support provided by Compute Canada. We appreciate the work of many researchers who are involved in the development of NuGrid computer codes that have been used in this study.

REFERENCES

Asplund M., Lambert D. L., Kipper T., Pollacco D., Shetrone M. D., 1999, *A&A*, **343**, 507

- Asplund M., Grevesse N., Sauval A. J., Scott P., 2009, *ARA&A*, **47**, 481
- Banerjee P., Qian Y.-Z., Heger A., 2018, *ApJ*, **865**, 120
- Bersillon O., Günsing F., Bauge E., Jacqmin R., Leray S., 2007, in *TALYS-1.6: Proceedings of the International Conference on Nuclear Data for Science and Technology*, EDP Sciences, Nice, France.
- Bertolli M. G., Herwig F., Pignatari M., Kawano T., 2013, preprint, ([arXiv:1310.4578](https://arxiv.org/abs/1310.4578))
- Busso M., Gallino R., Wasserburg G. J., 1999, *ARA&A*, **37**, 239
- Campbell S. W., Lugaro M., Karakas A. I., 2010, *A&A*, **522**, L6
- Clarkson O., Herwig F., Pignatari M., 2019, *MNRAS*, **488**, 222
- Cowan J. J., Rose W. K., 1977, *ApJ*, **212**, 149
- Cyburtt R. H., et al., 2010, *ApJS*, **189**, 240
- Dardelet L., et al., 2014, in *Proceedings of XIII Nuclei in the Cosmos (NIC XIII)*. 7-11 July, 2014. Debrecen, Hungary. Online at <http://pos.sissa.it/cgi-bin/reader/conf.cgi?confid=204>. p. 145
- Denissenkov P. A., Herwig F., Battino U., Ritter C., Pignatari M., Jones S., Paxton B., 2017, *ApJ*, **834**, L10
- Denissenkov P., et al., 2018, *Journal of Physics G*, **45**, 055203
- Denissenkov P. A., Herwig F., Woodward P., Androssy R., Pignatari M., Jones S., 2019, *MNRAS*, **488**, 4258
- Fujiya W., Hoppe P., Zinner E., Pignatari M., Herwig F., 2013, *ApJ*, **776**, L29
- Hampel M., Stancliffe R. J., Lugaro M., Meyer B. S., 2016, *ApJ*, **831**, 171
- Herwig F., Pignatari M., Woodward P. R., Porter D. H., Rockefeller G., Fryer C. L., Bennett M., Hirschi R., 2011, *ApJ*, **727**, 89
- Herwig F., Woodward P. R., Lin P.-H., Knox M., Fryer C., 2014a, *ApJ*, **792**, L3
- Herwig F., Woodward P. R., Lin P.-H., Knox M., Fryer C., 2014b, *ApJ*, **792**, L3
- Jadhav M., Pignatari M., Herwig F., Zinner E., Gallino R., Huss G. R., 2013, *ApJ*, **777**, L27
- Jones S., Ritter C., Herwig F., Fryer C., Pignatari M., Bertolli M. G., Paxton B., 2016, *MNRAS*, **455**, 3848
- Käppeler F., Gallino R., Bisterzo S., Aoki W., 2011, *Reviews of Modern Physics*, **83**, 157
- Karakas A. I., Marino A. F., Nataf D. M., 2014, *ApJ*, **784**, 32
- Liu N., et al., 2014, *ApJ*, **786**, 66
- Lugaro M., Karakas A. I., Stancliffe R. J., Rijs C., 2012, *ApJ*, **747**, 2
- Lugaro M., Campbell S. W., Van Winckel H., De Smedt K., Karakas A. I., Käppeler F., 2015, *A&A*, **583**, A77
- Mishenina T., et al., 2015, *MNRAS*, **446**, 3651
- Pignatari M., et al., 2016, *ApJS*, **225**, 24
- Rauscher T., Thielemann F.-K., 2000, *Atomic Data and Nuclear Data Tables*, **75**, 1
- Roederer I. U., et al., 2012, *ApJS*, **203**, 27
- Roederer I. U., Cowan J. J., Preston G. W., Shectman S. A., Sneden C., Thompson I. B., 2014a, *MNRAS*, **445**, 2970
- Roederer I. U., et al., 2014b, *ApJ*, **791**, 32
- Roederer I. U., Karakas A. I., Pignatari M., Herwig F., 2016, *ApJ*, **821**, 37
- Shingles L. J., Doherty C. L., Karakas A. I., Stancliffe R. J., Lattanzio J. C., Lugaro M., 2015, *MNRAS*, **452**, 2804
- Thielemann F. K., et al., 2011, *Progress in Particle and Nuclear Physics*, **66**, 346

APPENDIX A: COMPARISON OF PREDICTED AND OBSERVED ABUNDANCES

For the comparison in Figure 4 we have used the standard spectroscopic ratios of the observed abundances in the star

HD94028

$$[A/Fe]_{\text{obs}} = \log_{10} \frac{X_{A,\text{obs}}}{X_{A,\odot}} - \log_{10} \frac{X_{\text{Fe,obs}}}{X_{\text{Fe},\odot}},$$

where X_A is the mass fraction of an element A. Their theoretical counterparts are

$$[A/Fe]_{\text{theor}} = \log_{10} \frac{X_{A,\text{theor}}}{X_{A,\odot}} - \log_{10} \frac{X_{\text{Fe,theor}}}{X_{\text{Fe},\odot}},$$

where

$$X_{A,\text{theor}} = dX_{A,\text{ipr}} + (1-d)X_{A,\text{BKG}},$$

assuming that a fraction d of the abundances $X_{A,\text{ipr}}$ from an i-process nucleosynthesis site had been mixed with a $(1-d)$ fraction of some background (BKG) abundances $X_{A,\text{BKG}}$ in the inter-stellar medium (ISM) or in the i-process source before that mixture was accreted by the star. Therefore, the theoretical abundances depend on the assumed background and initial abundances $X_{A,\text{init}}$.

A1 The pinning method

The predicted abundances in Figure 4 are computed under the assumptions that $X_{A,\text{init}} \propto X_{\text{Fe,obs}}$ and $X_{A,\text{BKG}} = 0$, as for the Population-III ISM. We also assume that $X_{\text{Fe,theor}} = X_{\text{Fe,init}} = X_{\text{Fe,obs}}$, because the strong depletion of the Fe abundance in Figure 3 is an artefact of our one-zone nucleosynthesis simulation, while in a multi-zone He shell of a real stellar i-process site the Fe seed nuclei are replenished by convective mixing. In this case, we have

$$[A/Fe]_{\text{theor}} = \log_{10} d + \log_{10} \frac{X_{A,\text{ipr}}}{X_{A,\text{init}}}.$$

The $[A/Fe]_{\text{theor}}$ distribution is then normalized (pinned) to an element B using a normalization factor d , such that $[B/Fe]_{\text{theor}} = [B/Fe]_{\text{obs}}$.

A2 The dilution method

If we assume that $X_{A,\text{init}}$ is still proportional to $X_{\text{Fe,obs}}$, but $X_{A,\text{BKG}} = X_{A,\text{init}}$ and $X_{\text{Fe,theor}}$ is now computed like the abundances of all other elements then

$$[A/Fe]_{\text{theor}} = \log_{10} \frac{\left[d \frac{X_{A,\text{ipr}}}{X_{A,\odot}} + (1-d) \frac{X_{A,\text{init}}}{X_{A,\odot}} \right]}{\left[d \frac{X_{\text{Fe,ipr}}}{X_{\text{Fe},\odot}} + (1-d) \frac{X_{\text{Fe,init}}}{X_{\text{Fe},\odot}} \right]}.$$

In this case, the factor d plays the role of a dilution coefficient in mixing of the i-process abundances with the same initial abundances that were used in the i-process nucleosynthesis simulations. This method is more suitable for a situation when the i-process abundances were accreted locally from a binary or stellar cluster companion of the star. The best-fit theoretical abundance distribution from Figure 4 is plotted in Figure A1 using the dilution method. The important difference between the two comparison methods is that only the pinning method can provide negative theoretical abundances that sometimes are actually observed, like the Cu and Ge abundances in HD94028.

This paper has been typeset from a $\text{\TeX}/\text{\LaTeX}$ file prepared by the author.

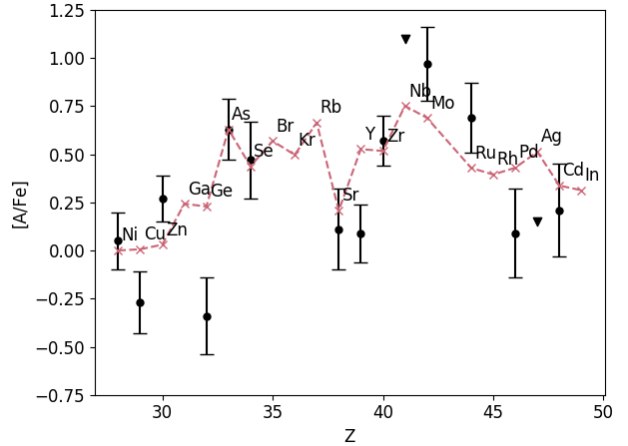


Figure A1. Same as the brown-dashed curve in Figure 4, but using the dilution abundance comparison method.